Title

Multifunctional light beam source for surface slope measuring long trace profilers

ISBN

978-1-5106-3790-0

Authors

Yashchuk, Valeriy V

Lacey, Ian

Anderson, Kevan

et al.

Publication Date

2020-08-21

DOI

10.1117/12.2570462

Peer reviewed

Multifunctional light beam source for surface slope measuring long trace profilers

Valeriy V. Yashchuk*[a], Ian Lacey[a], Kevan Anderson[a], Jeff Dickert[a], Brian V. Smith[a], and Peter Z. Takacs[a,b]

[a]Lawrence Berkeley National Laboratory, One Cyclotron Road, Berkeley, CA 94720, USA;
[b]Surface Metrology Solutions, LLC, 19 South First Street, B-901, Minneapolis, MN 55401, USA

ABSTRACT

To fully exploit the advantages of fourth-generation synchrotron light sources, diffraction-limited-storage-rings (DLSR) and fully coherent free electron lasers (FELs), beamline mirrors and diffraction grating must be of exceptional quality. To achieve the required mirror and grating quality, the metrology instrumentation and methods used to characterize these challenging optics and, even more so, optical assemblies must also offer exceptional functionality and performance. One of the most widely used slope measuring instruments for characterizing x-ray optics is the long trace profiler (LTP). The easily reconfigurable mechanical design of the LTP allows optimization of the profiler arrangement to the specifics of a particular metrology task. Here, we discuss the optical schematic, design, and performance of an original multifunctional light beam source that provides functional flexibility of the LTP optical sensor. With this source, the LTP can be easily reconfigured for measurements of x-ray mirrors or diffraction gratings that have widely different source coherence requirements. Usage of a source with a low degree of coherence for mirror metrology helps to suppress the LTP systematic errors due to spurious interference effects in the LTP optical elements. A high-coherence narrow-band source is used for groove-density-distribution characterization of x-ray diffraction gratings. The systematic error and spatial resolution of the LTP with the different sources is also measured and analyzed.

Keywords: x-ray optics, optical metrology, surface slope profilometry, LTP, pencil beam interferometry, light beam source, optical sensor, error reduction

1. INTRODUCTION

To fully exploit the advantages of the fourth-generation synchrotron light sources, diffraction-limited-storage-rings (DLSR) and fully coherent free electron lasers (FELs), beamline mirrors and diffraction grating must be of exceptional quality. Thus, mirrors with residual (after subtraction of an ideal shape) surface slope and height errors of < 50-100 nrad (root-mean-square, rms) and < 1-2 nm (rms), respectively, with tight requirements to the allowed power spectral density and correlation lengths of errors are absolutely essential in x-ray beamlines. In addition, for applications such as nano-focusing, the desired mirrors are significantly curved in the tangential (along the beam) direction with extremely high sagittal (across the beam) curvature, presenting formidable challenges to 3D full surface metrology. These requirements are for optics with lengths up to one meter and in face up, face down and sideways deflection orientations. The ex-situ metrology that supports the optimal usage of these optics at the beamlines must offer corresponding functionality and performance in measurements with the optics alone and, most challenging, with the optical assemblies (for a review, see, for example, Refs. [1-4] and references therein).

For surface slope measurements in the low spatial frequency range, the two most common instruments used at synchrotron facilities are the long trace profiler (LTP) [5-9] and the autocollimator (AC) based profiler such as the NOM system at HZB/BESSY-II [10,11]) and those at various other facilities [12-18]. In order to achieve the ultimate performance from these tools, they require advanced environmental conditions [19] and sophisticated data acquisition strategies to suppress random and drift errors [20-23]. Even so, the measurement accuracy is limited by the instrument's inherent systematic errors, which often are on the level of 1-2 μrad over the roughly 10 mrad dynamic measurement range. This has made vital the development of a variety of comprehensive and ingenious calibration methods for suppression of the systematic errors [24-31]. However, with the systematic error dependent on the peculiarities of the experimental set-up and the shapes and sizes of the optics under test [32], accurate calibration of the instruments is an arduous task. Therefore, we should try to minimize the systematic error via optimizing the profiler's design.

*VVYashchuk@lbl.gov; phone 1 510 495-2592; fax 1 710 486-7696; https://als.lbl.gov/people/valeriy-yashchuk/

The optical sensor of the NOM-like profilers, based on an industrial electronic AC ELCOMAT-3000 [33], is not accessible for modification and improvement at optics metrology labs of the x-ray light source facilities. Unlike the AC-based profilers, the open optical layout and mechanical design of the LTP are easily reconfigurable, which allows for optimization of the profiler arrangement to the specifics of a particular metrology task. For instance, when equipped with a single-mode laser light source, the LTP allows precision characterization of groove-density distribution of diffraction gratings [34-36]. This is impossible with the ELCOMAT-3000, which uses a broad-band non-coherent LED light source. Also, unlike the AC-based tools, the LTP profilers do not require a light-limiting aperture placed close to the SUT. This simplifies measurements with optical assemblies. Another example specifically for the Advanced Light Source (ALS) LTP-II gantry system [8,37,38], it has a capability for raising the LTP sensor above the optical bench to increase the space needed for measurements of large multi-component optical assemblies. Finally, there is still an open question about the possibility to control/monitor the LTP systematic errors when using the LTP in different operational modes, as first discussed in Ref. [37].

A few years ago, we started an R&D project on development of a new LTP optical sensor aimed at significantly improving performance. The activity in this direction was triggered by the need for a higher performing slope measuring system suitable for high accuracy metrology on optics for beamlines under development in the upgrade of the ALS to a DLSR facility [39,40]. Thus, using a comprehensive optical model of the LTP-II sensor, we have critically reanalyzed the common approaches to the LTP optical design. The preliminary results of the model simulations are discussed in other contribution to this conference [41].

In this paper, we discuss the optical schematic, design, and performance of an original multifunctional light beam source that gives additional functional flexibility to the LTP optical sensor (Sec. 2). With this source, the LTP can be easily reconfigured for measurements of x-ray mirrors or diffraction gratings. Usage of a light beam with a low degree of coherence for mirror metrology helps to suppress the LTP systematic errors due to spurious interference effects in the LTP optical elements (for a comprehensive discussion of the LTP systematic errors due to spurious interference effects, see Ref. [41]). The high-coherence narrow-band light beam is used for groove-density-distribution characterization of x-ray diffraction gratings. The performance of the LTP with different types of light beam sources is also analyzed based on the direct measurements of the profiler's systematic error (Sec. 3) and spatial resolution (Sec. 4). The paper concludes (Sec. 5) by summarizing the main concepts discussed through the paper and outlining a plan for future work.

2. THE ALS LTP-II UPGRADED WITH MULTIFUNCTIONAL LIGHT BEAM SOURCE

In this section, we briefly describe the design and major functionality of the LTP-II that is in operation at the ALS X-Ray Optics Laboratory (XROL) [19] (Sec. 2.1). Recently, the LTP-II was upgraded to allow easy switching between operational modes utilizing the output from a frequency-stabilized single-mode diode-laser (SMDL) and from a superluminescent light emitting diode (SLED) (Sec. 2.1). The LTP-II performance in the different modes of operation of the multifunctional light beam source (MFLS) is treated throughout this paper from the point of view of the instrument's systematic error and spatial resolution.

2.1 The optical design of the upgraded ALS LTP-II

The LTP-II optical sensor is based on the pencil beam interferometer, initially suggested and patented by K. Von Bieren in 1985 [42-44] and first applied in the long trace profiler for precision characterization of x-ray mirror surface slope topography in 1986 [5,6]. Having a number of important modifications [45-48] and revisions [9,38] to the optical schematic, LTP type profilers remain one of only two classes of surface slope measuring tools (together with the NOM-like profilers) that are broadly in use at metrology laboratories of x-ray facilities.

Figure 1 shows the current optical schematic of the ALS XROL LTP-II and the LTP-II experimental arrangement used for measurements with an elliptical mirror that is designated as the XROL reference ellipse.

The LTP-II sensor, with elements within the dotted box in Fig. 1(a), is mounted on an air-bearing translation carriage. In addition to the last upgrade described in Ref. [38], when the Dove prism in the reference channel was removed, the LTP-II is now equipped with the MFLS combining the SMDL and SLED light beam sources. The LTP-II operated with the output from the SMDL is used, in particular, to measure diffraction gratings in the manner discussed in Refs. [34-36] (see also other contribution to this conference [49]).

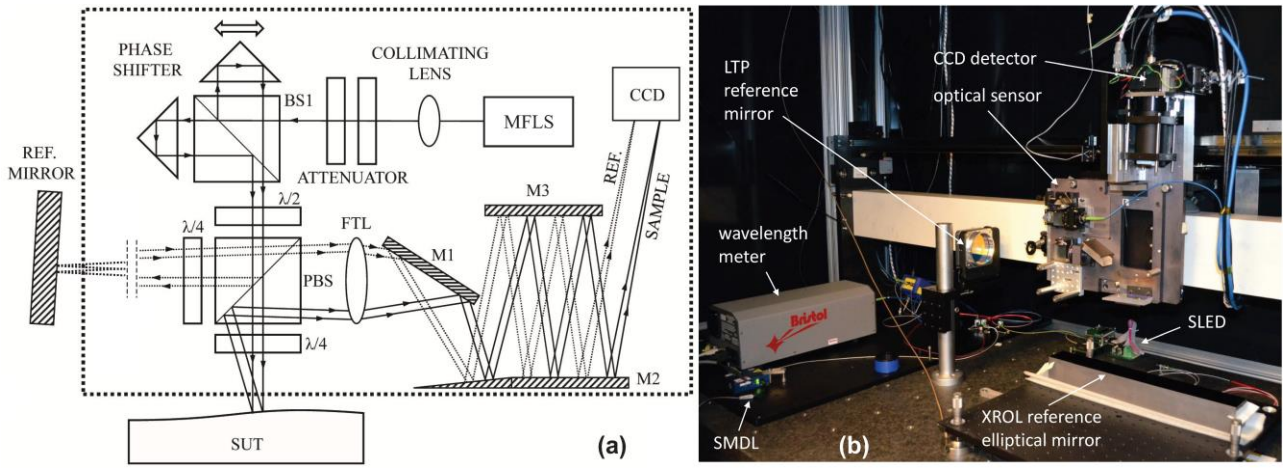

Figure 1. (a) Optical schematic of the ALS XROL LTP-II and (b) the LTP-II experimental arrangement used for measurements with a reference elliptical mirror (for notations, see the text).

The phase shifter [Fig. 1(a)], consisting of the movable and stationary Porro prisms, is used to adjust the phase difference and spatial separation of the two beam components, formed with a beam splitter BS1 [Fig. 1(a)]. The polarizing beam splitter PBS sends the two-component beams to the surface under test (SUT) in the sample arm and to the stationary reference mirror in the reference arm. The reference arm records a combination of spurious slope variations due to the carriage pitch wobbling and pointing instability of the laser beam.

In the original ALS LTP-II design [46], the Dove prism was used in the reference arm in order to give the spurious slopes due to the carriage pitch wobbling and light beam pointing instability the same relative phases so that a single subtraction would correct the SUT measurement of both error sources. However, as was pointed out in Ref. [38], the poor quality of the Dove prism is one of the major sources of the LTP-II systematic errors. Thus, the Dove prism was removed. Nevertheless, as it is demonstrated in Ref. [50], the LTP-II pointing instability error can be neglected if a multi-scan run, arranged according to the optimal scanning strategy [20,23], designed to defeat the measurement errors due to instrumental temporal drifts is carried out.

The reflected sample and reference beams are focused with the Fourier transform lens (FTL) onto a position sensitive CCD detector. In the LTP with a coherent light beam, the detected intensity distribution resulting from the interference of the two components of each beam, depends on the phase shift between the beam components. In the classical pencil beam interferometry (PBI) mode of the LTP with the phase difference adjusted to π, the interference has a destructive character with the intensity minimum in the center. The position of the central minimum is a measure of the SUT surface slope. The folding mirrors, M1, M2, and M3, are used to make a compact design at the FTL focal length of 1.25 m.

2.2 ALS LTP-II multifunctional light beam source

Figure 2 presents a schematic of the multifunctional light beam source [plots (a) and (b)] and shows the ALS LTP-II optical sensor with the beam shaping elements on the movable carriage [plot (c)].

In our case, the SMDL is a frequency-stabilized single-longitudinal-mode diode laser, equipped with a polarization maintaining fiber of the PANDA style [51]. The laser generates a light beam at the wavelength of 632.90 nm with an output power of 2.2 mW that is supplied to a Thorlabs 630-nm 1×2 single mode fiber optic splitters (FOS) with a 90:10 splitting ratio. The 10% output of the FOS is connected to a laser wavelength meter [52] that is specified to measure the absolute wavelength with an accuracy of ± 0.0008 nm. The light from the FOS 90% output goes to a Thorlabs 630-nm 2×1 single mode fiber optic couplers (FOC) with 50:50 coupling ratio. The second input of the FOC is connected to the SLED module [53,54] with a mean wavelength of 636.4 nm at the bandwidth of 5.7 nm. The FOC output is attached to a digital variable attenuator (DVA) [55], which provides controlled attenuation of the output optical power with a dynamic range of more than 4 orders.

All the MFLS elements listed above, are located on the LTP-II granite table. In order to bring the light to the LTP optical sensor, the output of the DVA is connected to a 630-nm polarization-maintaining single-mode patch cable (PM SM PC)

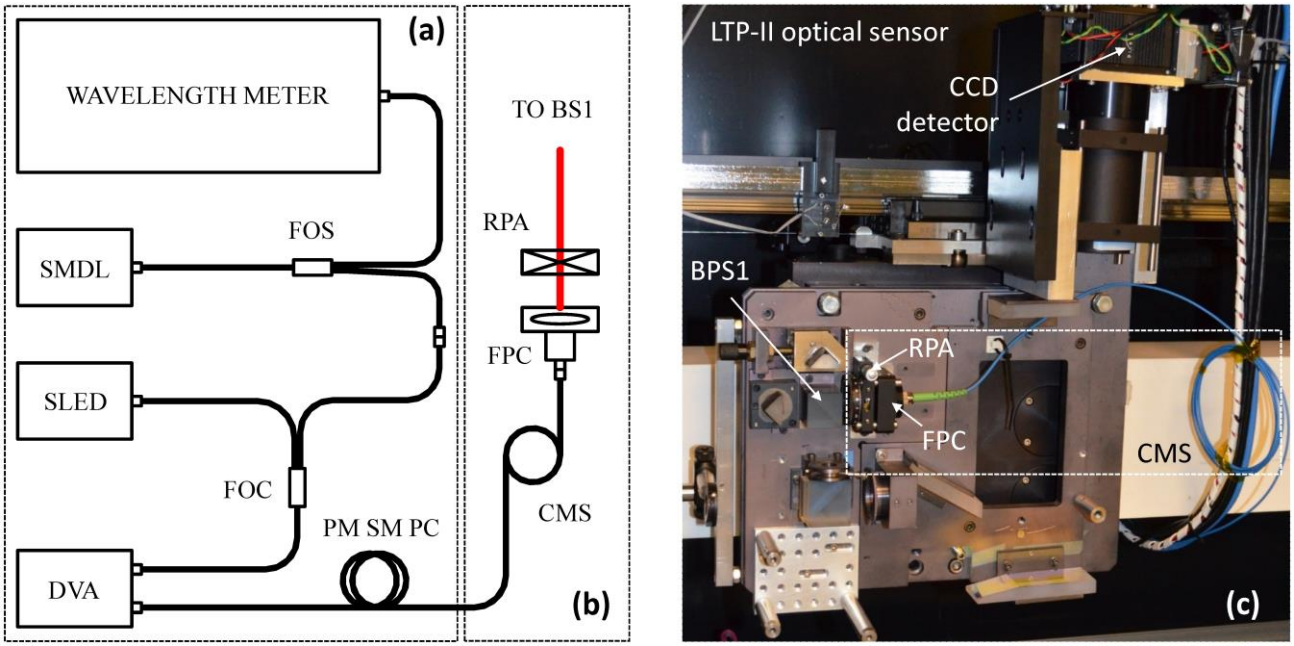

Figure 2 Schematic of the multifunctional light source: (a) the elements placed on the LTP-II granite table, (b) the beam shaping elements and shows the on the movable carriage. SMDL is the Single longitudinal Mode fiber-coupled Diode Laser, SLED is the superluminescent light emitting diode module; DVA is the digital variable attenuator; FOS is the 630-nm 1×2 single mode fiber optic splitters with splitting ration 90:10; FOC is the 630-nm 2×1 single mode fiber optic coupler with coupling ration 50:50; PM SM PC is the polarization-maintaining single-mode patch cable; CMS is the cladding mode suppressor made of 7 loops of the patch cable; FPC is the fiber-port collimator with five degrees of freedom plus rotation adjustment; RPA is the rotating polarizer attenuator. After the RPA, the light beam goes to the beam splitter BS1 of the LTP optical sensor (see also Fig. 1).

of PANDA style. The patch cable with the total length of 10 meter is placed to the LTP folding cable tray together with other cables, including the CCD camera signal and the power cables, as well as the cables for a Peltier-element based temperature stabilization system.

The end of the 10-m long patch cable that is downstream of the cladding mode suppressor (CMS), which is made of 7 turns of the patch cable, is attached to a Thorlabs fiber-port collimator (FPC) that is designed to provide micro-positioning alignment with five degrees of freedom plus rotation adjustment. The FPC adjustments are used to align the beam in the reference channel to be parallel to the translation axis of the LTP-II gantry system. The rotating polarizer attenuator (RPA) is needed to maintain the polarization direction of the light entering the LTP optical sensor. It is also useful if additional light intensity attenuation is desired.

Because of the carriage translation, the patch cable in the folding tray is the subject of continuous bending that is known to cause so-called ‘bend losses’ of the light power (see, for example, Refs. [56,57] and references therein). This is due to the coupling of the light from core modes (guided modes) to cladding modes, when fiber is bent. In the LTP application, the position of the fiber bending varies on the scale of a few meters, which can lead to a significant (a few orders of magnitude) fluctuation of the power of the output light. The power fluctuation can be suppressed with addition of a cladding mode suppressor that, in our case, is a stationary loop in the downstream part of fiber of 5-10 turns, labeled in Fig. 2 as ‘CMS.’

Unfortunately, even with the CMS added, we need to use active stabilization of the LTP light-beam intensity with the DVA. The stabilization that uses the integrated intensity of the detected light as a feedback signal is one of the functions of the LTP-II motion control and data acquisition (MCDA) system. The MSDA system also provides for automated control and monitoring of all major parameters of the SMDL, SLED, and DVA. In the case of the SMDL light beam, we additionally record in the measurement data file the temporal variation of the light wavelength.

As an illustration of the high performance of the MFLS discussed in this section, Fig. 3 reproduces the temporal variation of the SMDL light wavelength as measured with the wavelength meter during a 6-hour long LTP-II run. This high degree of the wavelength stability of ~ 10^{-6} is required for precision characterization of groove density variation of x-ray diffraction gratings. Application of the XROL LTP-II for measurements with variable-line-spacing (VLS) grating is discussed in Ref. [49].

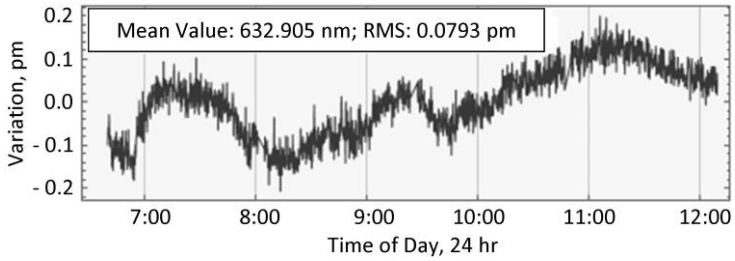

Figure 3. Temporal variation of the SMDL light wavelength during a 6-hour long LTP-II measurement run.

2.3 Modes of operation available with the ALS LTP-II

The current design of our LTP-II allows us to change the profiler configuration to realize the single beam operation by simply placing a beam-stop between the BS1 and the upper Porro prism. As a result, four different arrangements are available with the ALS LTP-II with the MFLS, including the combinations of the single-beam (1B) and two-beam (2B) modes with the coherent and incoherent light from the SMDL and SLED. For the sake of brevity, we call these operational modes 1B-SMDL, 2B-SMDL, 1B-SLED, and 2B-SLED.

We should also take in to account the different algorithms for numerical evaluation of position of the intensity distribution of the detected light beam that is used as a measure of the SUT slope. For 1B arrangements, we use two algorithms. One algorithm calculates the centroid of the intensity distribution. We call this the centroid calculation positioning (CCP) algorithm. The other algorithm calculates the position of the maximum of the best-fit Gaussian distribution. This option is called the Gaussian maximum fit (GMF). Therefore, the operational modes of the LTP-II available with one-beam arrangements are 1B-SMDL/CCP, 1B-SLED/CCP, SMDL/GMF, 1B-SLED/GMF. Here, we try to follow to the notations used in Ref. [50].

In the case of two-beam arrangements, the detected intensity distributions are very different for the 2B-SMDL and 2B-SLED light beams – Fig. 4.

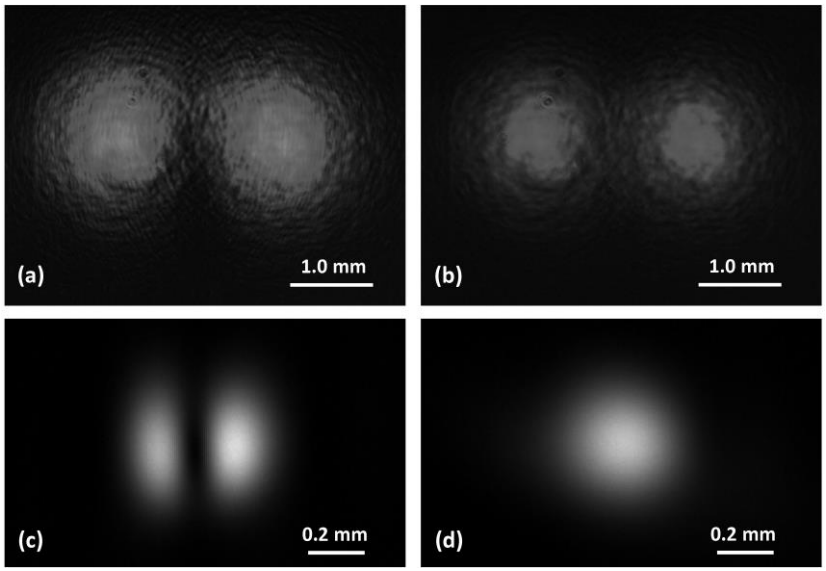

Figure 4. The light intensity distribution on the SUT (the top plots) and as detected with the LTP-II CCD (the bottom plots) in the case of the two-beam arrangement with the light beams from the SMDL (the left-hand plots) and from the SLED (the right-hand plots).

Due to the short spatial coherence of the SLED light, the interference effects in the detected intensity distribution of the 2B-SLED light beam are washed out, and the distribution has a single-peak shape. Therefore, for positioning the 2B-SLED light beam we still use the CCP and GMF algorithms. The 2B-SMDL mode of operation of the ALS LTP-II corresponds to the PBI-based LTP. In this case, the classical positioning algorithm consists in finding of the position of the minimum of the two-peak destructive interference intensity distribution. We call this mode of operation the 2B-SMDL/PBI mode. Additionally, the two-peak intensity distribution detected with the 2B-SMDL light beam can also be positioned with the CCP algorithm; this is the 2B-SMDL/CCP operational mode.

The availability of different modes of operation raises questions about their advantages and drawbacks, namely which one(s) give the most faithful representation of the surface slope. In this paper we investigate two fundamental properties determining the profiler's performance.

One property is the level of the systematic errors of the slope profiler in the single- and two-beam arrangements with the coherent and incoherent light beams. At first glance, due to the inherent differential character of the two-beam (PBI-like) sensor, such a tool should be less sensitive to the imperfections of the sensor optical elements. This question has been empirically investigated in a recent article [37], where a 4-peak mode of operation for the PBI-based LTP was first suggested and experimentally tested. It has been demonstrated that a significant suppression of the LTP systematic error is achievable when the surface slope trace is measured from an average of the two slope traces determined by the left and right side minima. This observation is still wanting for a thorough verification and comprehensive understanding. The LTP-II systematic errors with the SMDL and SLED light beams are examined in the measurements with a mirror used as a reference standard. Previous measurements with two other surface slope profilers available at the ALS XROL have characterized the reference standard surface slope variation with high accuracy (see Sec. 3).

The other fundamental property of a slope profiler determining its operational performance is the spatial resolution, described by the instrument transfer function (ITF). Comparison of the spatial resolutions of the LTP-II in different operational modes is one of the major goals of the present investigation (see Sec. 4).

3. SYSTEMATIC ERROR OF THE ALS LTP-II UPGRADED WITH THE MFLS

In this section, we present the results of the systematic error tests performed with the LTP-II in different operational modes described in Sec. 2.3, when the tool is used for surface slope metrology with a standard reference mirror available at the XROL. The standard mirror with dimensions of 400 mm (length) × 50 mm (width) × 50 mm (thickness) has an elliptical shape determined by the conjugate parameters $R_1 = 22.5\,\text{m}$, $R_2 = 1.5\,\text{m}$ that are the distances from the mirror center to the ellipse foci, with a grazing incidence angle of $\theta = 10\,\text{mrad}$ at the mirror center. The total slope variation over the mirror clear aperture of 378 mm × 11 mm is about 8.9 mrad, covering almost the entire dynamic range of the LTP-II that is about 10 mrad. The tests consist of comparing the measurements with the LTP-II in a particular operational mode with the mirror inherent shape precisely measured with the Optical Surface Measuring System (OSMS) [18,23] and Developmental LTP (DLTP) [12,16] both available at the ALS XROL.

3.1 Surface slope characterization of the XROL reference elliptical mirror with the OSMS and DLTP

Figures 5 and 6 present the residual (after subtraction of the specified elliptical shape) surface slope variation (surface slope error) of the standardreference mirror as measured with the OSMS and DLTP. For the measurements, the ELCOMAT-3000 autocollimators in the OSMS and DLTP sample arms were equipped with circular apertures of 2.5-mm diameter.

The high confidence of the measurements is ensured by the application of a number of original experimental techniques for suppression of random, drift, and systematic errors of the measurements; as well as by the usage of special analytical methods and software for data analysis and processing (see Refs. [20,23,25] and references therein).

Indeed, in spite of the fundamental difference of the schematics of these profilers, where the OSMS AC is mounted directly to the translating carriage and the stationery DLTP utilizes a scanning pentaprism, the difference of the measurements is only about 80 nm (rms) – see Fig. 7. Half of the rms difference in Fig. 7 can be used as an estimation of the measurement accuracy of the mirror surface slope trace averaged over the two measurements shown in Figs. 5 and 6. In the LTP-II systematic error tests discussed in the Secs. 3.2 and 3.3, below, the averaged trace is used as the mirror inherent surface slope variation.

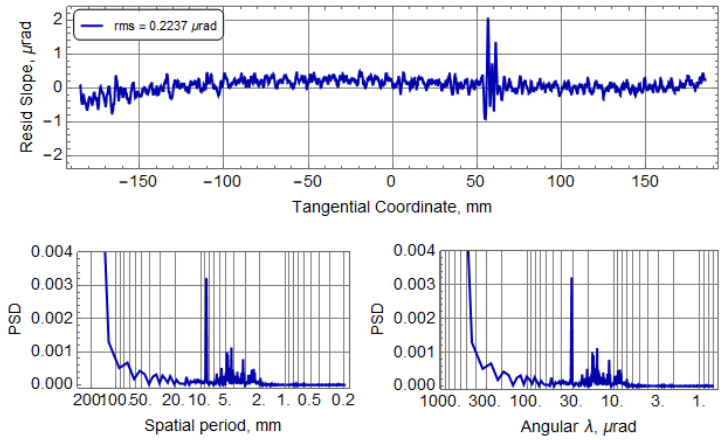

Figure 5. Residual (after subtraction of the specified elliptical shape) surface slope variation (the top trace) and the corresponding PSD distributions evaluated in the spatial and angular frequency domains (the bottom plots) of the reference elliptical mirror. The measurements were performed with the OSMS.

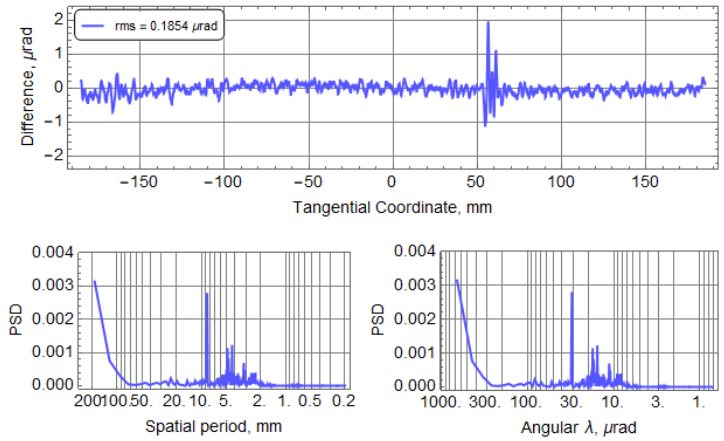

Figure 6. Residual (after subtraction of the specified elliptical shape) surface slope variation (the top trace) and the corresponding PSD distributions evaluated in the spatial and angular frequency domains (the bottom plots) of the reference elliptical mirror. The measurements were performed with the ALS XROL DLTP.

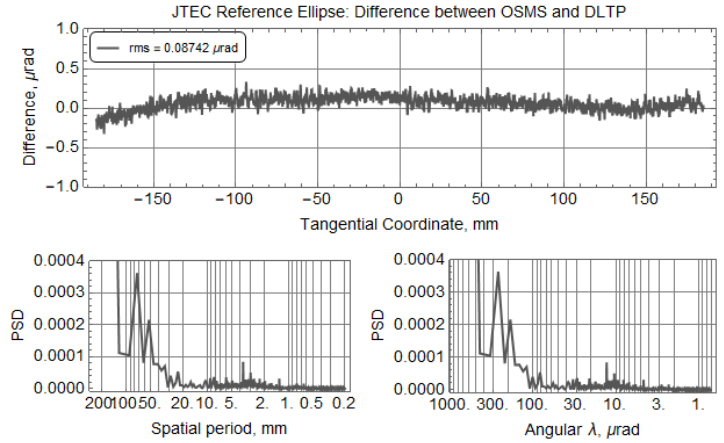

Figure 7. The difference of the surface slope variations (the top trace) and the corresponding PSD distributions evaluated in the spatial and angular frequency domains (the bottom plots), measured with the reference elliptical mirror using the XROL OSMS and DLTP.

In both measurements depicted in Figs 5 and 6, the slope error revels a quasi-periodic component with a period of about 8.5 mm, clearly seen in the power spectral density (PSD) distributions evaluated in the spatial and angular frequency domains. Such quasi-periodic error is characteristic of most deterministic polishing processes used for fabrication of aspherical x-ray optics [11,58,59]. There is also a local surface perturbation, seen near the tangential position of +60 mm. In the application of the mirror as a standard reference optic, this perturbation appears to be useful as a fiducial.

3.2 Systematic errors of the LTP-II in the single-beam arrangements

Figure 8 presents the results of surface slope metrology of the reference elliptical mirror carried out with the LTP-II in the single-beam arrangement with the SMDL and SLED light sources. The difference between the LTP-II measurement and the reference standard's surface topography, obtained by averaging the OSMS and DLTP measurements in Figs. 5 and 6, is shown in Fig. 9.

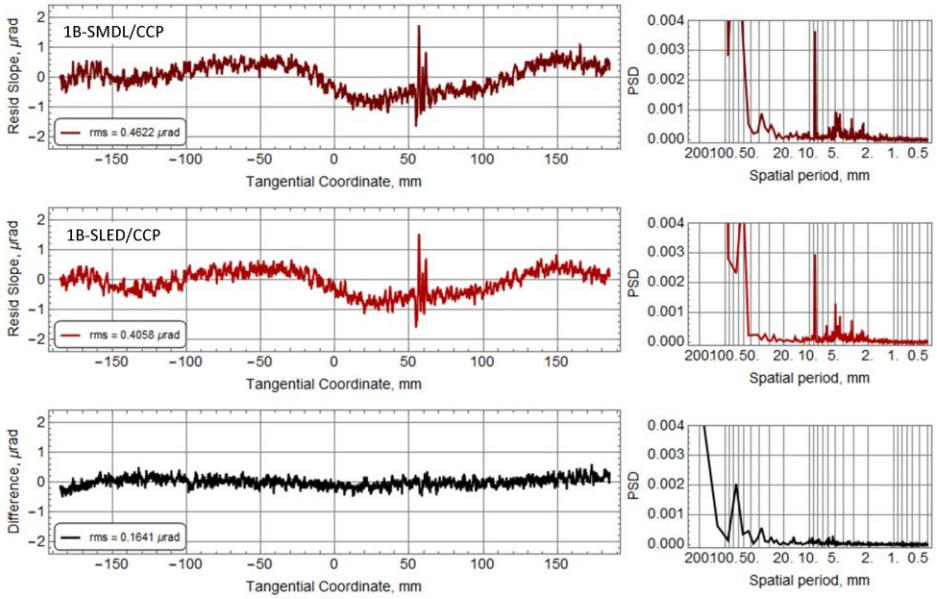

Figure 8. Residual (after subtraction of the specified elliptical shape) surface slope variation and the corresponding PSD distributions evaluated in the spatial frequency domains of the reference elliptical mirror as measured with the ALS LTP-II in the (a) 1B-SMDL/CCP and (b) 1B-SLED/CCP mode of operation; and (c) the difference of the slope measurements in plots (a) and (b) and its PSD distributions evaluated in the spatial frequency domains.

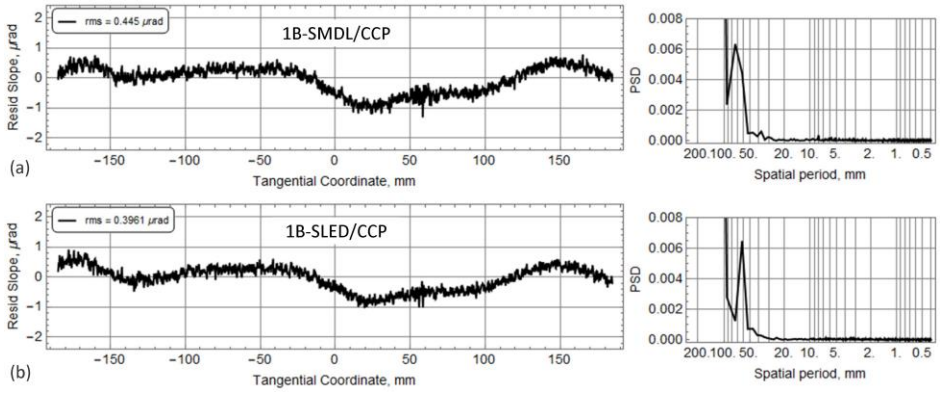

Figure 9. Systematic errors of the ALS LTP-II in the (a) 1B-SMDL/CCP and (b) 1B-SLED/CCP mode of operation, when measuring the reference elliptical mirror, and the corresponding PSD distributions evaluated in the spatial frequency domains. The systematic errors are found by subtracting the measured slope variations depicted in Fig. 8 of the reference surface topography obtained by averaging the OSMS and DLTP measurements in Figs. 5 and 6.

In the case of the LTP-II measurements in Figs. 8 and 9, the CCP algorithm has been used for determining the position of the detected light intensity distribution on the detector. Both operational modes, 1B-SMDL/CCP and 1B-SLED/CCP,

are capable of correctly reproducing the higher spatial frequency peculiarities of the mirror surface topography (compare with the reference surface slope data for the mirror as measured with the OSMS and DLTP and shown in Figs. 5 and 6). However, in both cases, there is a significant component of the LTP-II systematic error (Fig. 9) seen as a slope variation at the lower spatial frequencies. The overall shape of the systematic errors is the same. However, as indicated by the rms values of the slope error of 0.445 μrad (rms) and 0.396 μrad (rms) for the 1B-SMDL/CCP and 1B SLED/CCP, respectively, the error amplitude is slightly lower for the LTP-II in the 1B-SLED/CCP operational mode. The difference of the rms variation is really due to the difference of the high frequency random noise in the LTP-II measurements that is seen in the different levels of the random PSD variations at periods shorter than 20 mm in plots (a) and (b) in Fig. 9.

Figure 10 depicts the results of the application of the Gaussian maximum fitting, GMF, positioning algorithm to the same recorded images of the detected beam light intensity distributions as used to get the surface slope data depicted in Figs. 8 and 9. In this case, the measured rms surface error looks significantly better, 0.289 μrad (rms) and 0.257 μrad (rms) compared to 0.462 μrad (rms) and 0.406 μrad (rms) (see Fig. 8). However, the improvement is associated with the noticeable decrease of the spatial resolution resulted, for example, in the significantly reduced slope variation for the 'fiducial' perturbation near the 60-mm position. This is a remarkable effect that we investigate in more detail in Sec. 4.

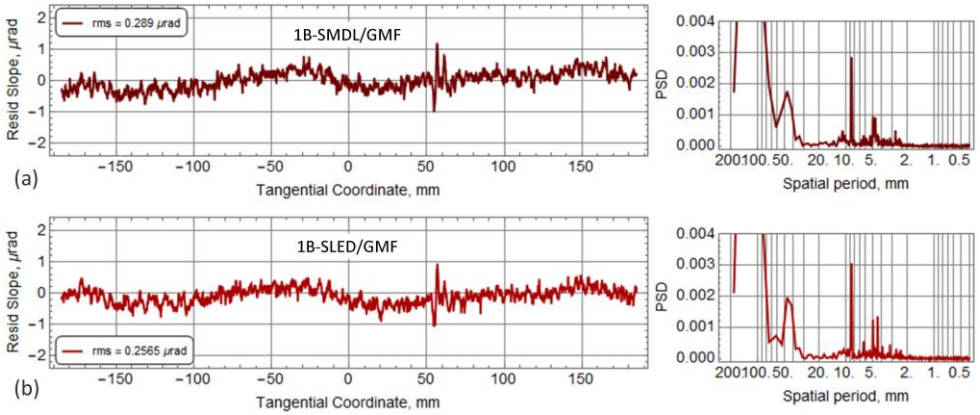

Figure 10. Residual (after subtraction of the specified elliptical shape) surface slope variation and the corresponding PSD distributions evaluated in the spatial frequency domains of the reference elliptical mirror as measured with the ALS LTP-II in the (a) 1B-SMDL/GMF and (b) 1B-SLED/GMF modes of operation.

3.3 Systematic errors of the LTP-II in the two-beam arrangements

Figures 11 and 12 present the results of surface slope measurements with the reference elliptical mirror performed with the LTP-II in two-beam arrangements, when equipped with the SLED (Fig. 11) and the SMDL (Fig. 12) light sources.

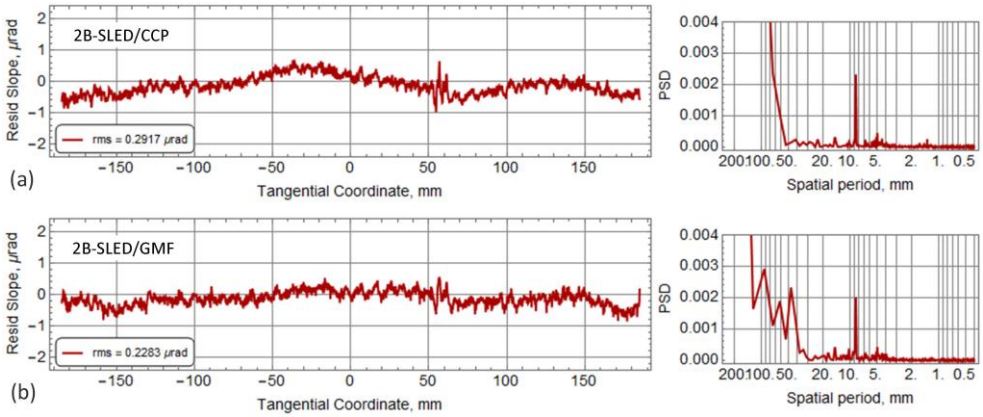

Figure 11. Residual (after subtraction of the specified elliptical shape) surface slope variation and the corresponding PSD distributions evaluated in the spatial frequency domains of the reference elliptical mirror as measured with the ALS LTP-II in the (a) 2B-SLED/CCP and (b) 1B-SLED/GMF modes of operation.

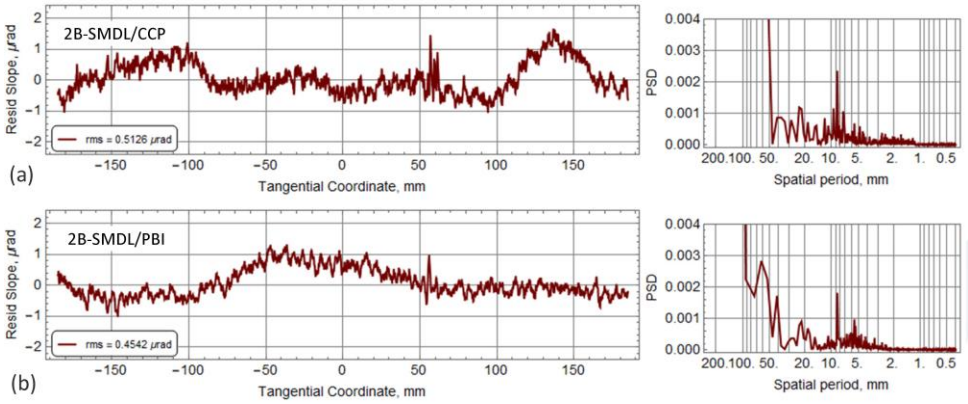

Figure 12. Residual (after subtraction of the specified elliptical shape) surface slope variation and the corresponding PSD distributions evaluated in the spatial frequency domains of the reference elliptical mirror as measured with the ALS LTP-II in the (a) 2B-SMDL/CCP and (b) 1B-SMDL/PBI modes of operation.

The major distinguishing feature of this set of measurements is the absence of a similarity of the low spatial frequency slope variation that is the contribution of the tool's systematic error. This is probably due to the additional sensitivity of the measurements to the relative phase between the two beams that is also sensitive to the imperfections of the LTP-II optical elements.

Similar to the single-beam arrangement, the overall systematic error that in Figs. 11 and 12 correlates with the rms variation of the measured residual slope, is larger for the operational modes with calculation of the centroid position, CCP. The correlation between the value of the systematic error and amplitude of the slope variation for the 'fiducial' perturbation near the 60-mm position larger, is one more evidence for the significant difference of the spatial resolution for these four modes of operation of the ALS LTP-II.

Concluding this section, we should acknowledge the principal difference between the data acquisition methods applied to the LTP-II measurements and to the OSMS and DLTP measurements for the high precision characterization of the XROL standard reference elliptical mirror. Unlike the OSMS and DLTP measurements, for the investigation of the LTP-II systematic errors in different operational modes, we used the data acquisition method based just on the optimal scanning strategy (OSS) that is good for suppression of the error related to the instrumental and set-up drifts [20]. This is fundamentally different from the data acquisition based on the advanced OSS (AOSS) [23] applied to the DLTP and OSMS measurements to additionally suppress the contribution of the systematic errors of the instruments. Application of the AOSS to the LTP-II measurements should also be beneficial for suppression of the tool's systematic error.

4. SPATIAL RESOLUTION OF THE ALS LTP-II UPGRADED WITH THE MFLS

Strictly speaking, the limited spatial resolution of a measuring instrument should be thought of as a source of instrumental systematic error. However, the influence of spatial resolution on the result of measurements is more appropriately investigated in the spatial frequency domain, requiring methods and reference (test) surfaces significantly different from those used in systematic error measurements in the angular domain, as discussed in Sec. 3. Therefore, we distinguish spatial resolution as a separate class of the instrumental properties affecting the ability of the instrument to correctly reproduce the amplitudes and phases of the quasi-periodical surface perturbations.

The spatial resolution properties of a slope measuring profiler can be characterized by the instrument's point spread function (PSF) that describes its response to a point (delta-function-like) slope topographic object (see, for example, Refs. [50,59] and references therein). A 1D surface slope profile measured with the OSMS can be expressed as a convolution of the PSF with the slope trace $\alpha_{SUT}(x)$, corresponding to the inherent (unperturbed by the measurement) topography of the SUT:

$$\alpha_{MES}(x) = PSF(x) * \alpha_{SUT}(x) + \varepsilon_{MES}(x), \tag{1}$$

where x is the position variable, $\alpha_{MES} \equiv \alpha_{MES}(x)$ is the measured trace, and the symbol '*' denotes the convolution operation. The noise term $\varepsilon_{MES}(x)$ describes the random errors of the measurement, arising, for example, due to the air

convection along the optical paths of the light beam [60]. For simplicity of the discussion in this section, we assume that measurement drift and angular systematic errors are negligible.

In the spatial frequency domain, the resolution properties of the instrument are described with the instrument's transfer function $ITF(u)$ defined as the Fourier transform ($\mathfrak{F}[\ldots]$) of the PSF,

$$ITF(u) = \mathfrak{F}[PSF(x)], \tag{2}$$

where u is the spatial frequency variable.

The for precise measurement of the ITF of a slope profiler, we apply a recently developed method based on test surfaces with one-dimensional (1D) linear chirped height profiles of constant slope amplitude [61-63].

The resolution properties of the ALS LTP-II equipped with the SMDL light source has been thoroughly investigated in our recent article [50]. Therefore, here we only briefly recall the major results of this work that have direct relation to the topic of the present paper (Sec. 4.1). The new results of the spatial resolution properties of the ALS LTP-II equipped with the SLED are presented in Sec. 4.2.

4.1 Spatial resolution of the LTP-II with the single-mode diode-laser, SMDL, light source

In the single-beam arrangement of the LTP-II, its spatial resolution is limited by the shape and size of the light beam incident to the SUT, defining the PSF of the tool. The LTP-II PSF in the 1B SMDL arrangement is approximately described with a Gaussian distribution

$$PSF(x) = \left(2\pi\sigma^2\right)^{-1/2} \exp\left(-x^2/(2\sigma^2)\right), \tag{3}$$

where σ^2 is the Gaussian variance parameter.

According to the measurements in Ref. [50], for the LTP-II operating in the 1B SMDL/CCP mode, $\sigma = 0.463$ mm, which is significantly smaller than the value $\sigma = 0.641$mm measured with the LTP-II in the 1B SMDL/GMF mode. The smaller value of the standard deviation corresponds to higher spatial resolution, which is in the perfect concordance with the observed difference of the fiducial feature amplitudes measured with the LTP-II in the single-beam arrangement (compare Figs. 8 and 10).

At first glance, for the case of the LTP-II in the two-beam arrangement, it is natural to use the PSF in the form of two shifted Gaussian functions, describing the intensity distribution in the two-component sample and reference beams:

$$PSF_{2G}(x) = A_- \exp\left(-(x-x_0)^2/(2\sigma_-^2)\right) + A_+ \exp\left(-(x+x_0)^2/(2\sigma_+^2)\right), \tag{4}$$

where x_0 is the parameter of the beam-component position shift, A_- and A_+ are the normalized intensities, and σ_-^2 and σ_+^2 are the variances of the beam components shifted in the negative and positive directions.

However, as demonstrated in Ref. [50], the two-component PSF given with Eq. (4) works well only to describe the resolution measurements with the LTP-II in the 2B SMDL arrangement when the CCP positioning algorithm is applied. In this case, the values of the parameters of the PSF in the form of the two-component Gaussian function are: $\sigma_- = \sigma_+ = 0.416$ mm, $x_0 = 0.958$ mm, and $A_-/A_+ = 0.81$. The latter two parameters have a strong dependence on the lateral shift of the two beam formed with the Porro-prism phase shifter (Fig. 1).

The ITF corresponding to $PSF_{2G}(x)$ has a π phase reversal at to the spatial period of the chirped sample of ~ 3.5 mm [49]. In LTP-II surface slope measurements, the SUT surface slope variations with the periods corresponding to the reversed phase of the ITF are reproduced with the reversed amplitudes. The π phase reversal is the known signature of an ITF with regions of negative amplitude (see, for example Refs. [64-66]).

A remarkable result of Ref. [50] is the experimental demonstration that, in the case of the LTP-II in the 2B SMDL/PBI mode of operation (utilizing the position of the central minimum of the detected two-peak fringe pattern determined by second-order-polynomial fitting of the central minimum in the pattern), the modeling of the ITF in the form of the two-component Gaussian-function does not work. Instead, the single Gaussian-function PSF [Eq. (3)] works well to describe the resolution measurements with the LTP-II in this operational mode [50]. In the arrangement of the LTP-II in

Ref. [50], the effective value of the standard deviation of the Gaussian-function PSF is $\sigma = 0.772$ mm. The larger value of the standard deviation corresponds to the smaller amplitude of the fiducial feature in Fig. 12(b) compared to that recorded in the single-beam arrangement, depicted in Fig. 8.

4.2 Spatial resolution of the LTP-II with the superluminescent light emitting diode, SLED, light source

In this section, we compare the spatial resolution of the LTP-II equipped with the SLED light source with the results of the resolution measurements with the LTP-II utilizing the SMDL light source [50] (see also Sec. 4.1).

Figure 13 shows the light intensity images recorded at the location of the SUT for the single-beam LTP-II arrangements operating with the SLED and SMDL light sources. The corresponding 1D distributions that are the fundamental physical quantities determining the profiler's PSF are also show. Similar data for the two-beam arrangement of the LTP-II with the SLED and SMDL light sources is presented in Fig 14.

The data in Figs. 13 and 14 correspond to the exactly the same geometrical arrangements of the LTP-II and have been recorded immediately before the spatial resolution measurements were performed with the chirped test sample. This validates with high confidence the results of the cross-comparison tests with the SLED and SMDL light sources.

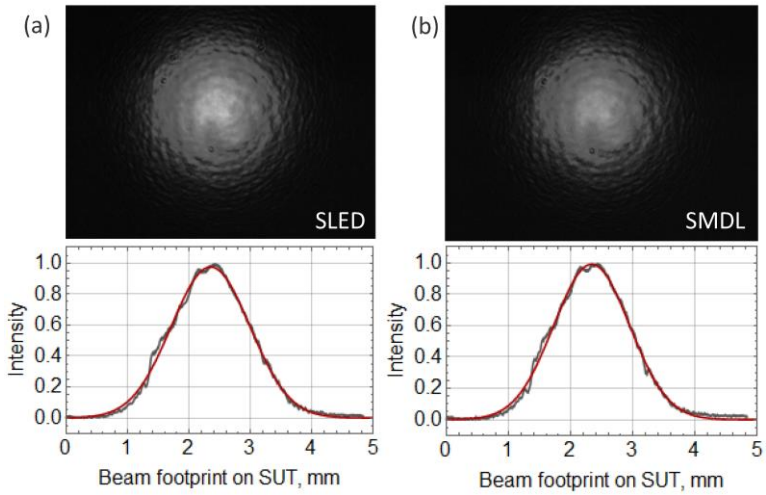

Figure 13. The light intensity distribution on the SUT for the single-beam arrangement of the LTP-II operating with the SLED (the left-hand plots) and SMDL light sources (the right-hand plots). The Gaussian fits are shown with the red lines.

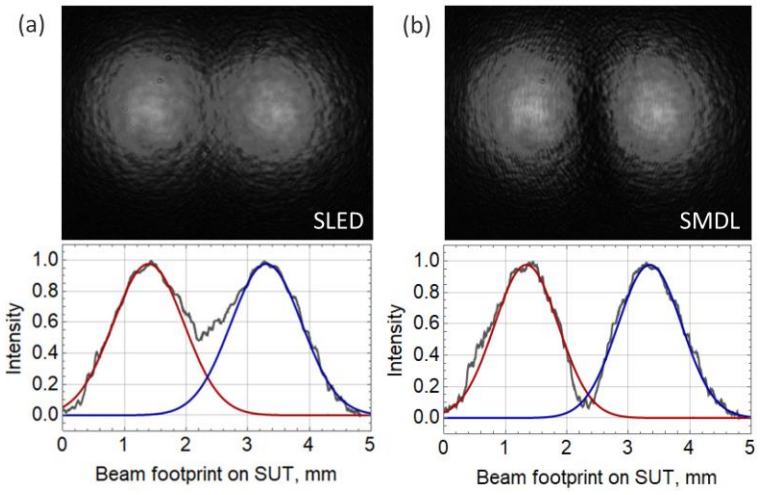

Figure 14. The light intensity distribution on the SUT for the two-beam arrangement of the LTP-II operating with the SLED (the left-hand plots) and SMDL light sources (the right-hand plots). The two Gaussian beam model best fits the measured distributions are shown with the red and blue solid lines.

The 1D distributions of the single-beam light intensities on the SUT shown in Fig. 13 are modeled with a Gaussian distribution with the standard deviations $\sigma = 0.64$ mm for the SLED beam and $\sigma = 0.61$ mm for the SMDL beam. The 1D distributions of the two-beam light intensities can be modeled with two laterally shifted Gaussian distributions (as shown in Fig. 14) found for the single beams. The values of the shift extracted from the fit are $x_0 = 0.955$ mm for the 2B SLED light beam and $x_0 = 1.005$ mm for the 2B SMDL light beam.

Figure 15a shows with the solid blue line the slope profile of the chirped test sample [59-61] measured with the LTP-II in the 1B SLED/CCP operational mode. The data acquisition and processing procedures are the same as described in Ref. [50]. The effect of the limited spatial resolution of the profiler is seen in Fig. 15a as a characteristic deviation (increasing with decreasing oscillation period) of the measured oscillation amplitudes from the slope profile inherent to the sample (shown in Fig. 15a with the dotted black line).

The comparison of the spatial calibrations of the LTP-II in the 1B SLED/CCP and 1B SMDL/CCP operational modes is given in Fig. 15b with the overlapped chirped-test-sample slope profiles measured with the SLED and SMDL light beams, shown with the dashed blue and dotted blue lines, respectively. The chirped-test-sample slope profiles measured with the SLED and SMDL light beams are practically indistinguishable. The effective value of the standard deviation that best fit the effective PSF function as a Gaussian distribution is $\sigma_{eff} = 0.467$ mm that is in perfect agreement with the result of Ref. [50] for a similar measurement with the LTP-II in the 1B SMDL/CCP operational mode (see also the relevant discussion in Sec. 4.1).

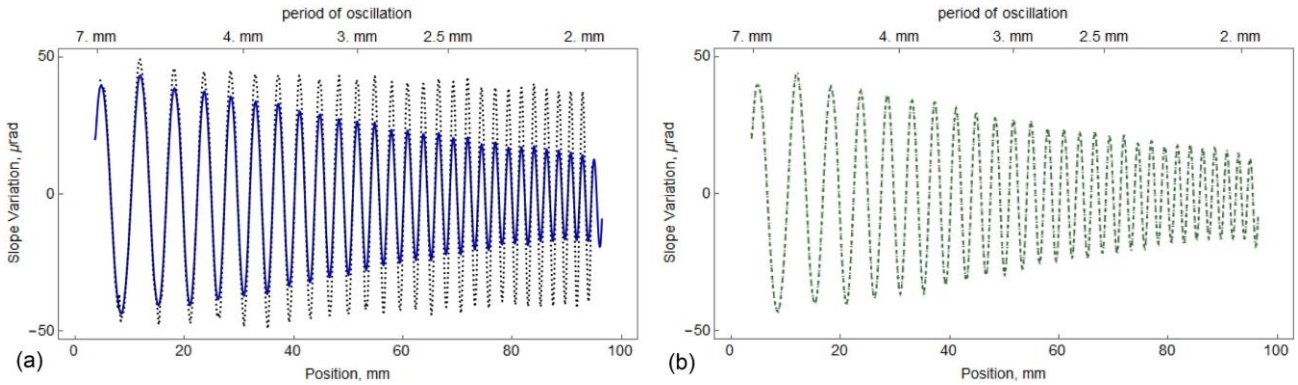

Figure 15. (a) Chirped test sample slope profile measured with the LTP-II in the 1B SLED/CCP operational mode (the solid blue line); (the dotted black line) the inherent slope variation of the low-frequency pattern of the chirped sample as measured with a Fizeau interferometer with the effective pixel size of 0.1 mm [50]; (b) the same as in plot (a) slope profile measured with the LTP-II in the 1B SLED/CCP operational mode (the dashed blue line) overlapped with the result of a similar measurement with the LTP-II in the 1B SMDL/CCP operational mode (the dotted green line). The chirped-test-sample slope profiles measured with the SLED and SMDL light beams are practically indistinguishable.

We have also performed a comparison of the spatial calibrations of the LTP-II in the 1B SLED/GMF and 1B SMDL/GMF operational modes. Because of the lack of space, we omit here a detailed discussion of the obtained data. In summary, the comparison has revealed the almost perfect identity of the spatial resolution properties of the LTP-II in the 1B SLED/GMF and 1B SMDL/GMF operational modes. In this case, the value of the standard deviation of the effective Gaussian-function PSF practically coincides with the given in Sec. 4.1, $\sigma = 0.641$mm.

Therefore, the spatial resolution of the LTP-II using a single-beam from the SLED light source also strongly depends on the data processing algorithm. Application of the CCP algorithm provides higher resolution than that of the GMF algorithm, applied to the same detected intensity distribution images. This conclusion is in excellent accord with the observed difference of the amplitudes of the fiducial feature on the surface of the XROL reference elliptical mirror discussed in Sec. 3 and depicted in Figs. 8b and 10b. Note that the measured amplitude of the quasi-periodic surface perturbation with the spatial period of ~8.5 mm does not depend on the mode of operation of the LTP-II in the single beam arrangement. This is clearly seen from comparison of the corresponding PSD spectra in Figs. 8 and 10. Indeed, as indicated in Fig. 15, in this case, the ITF function is almost equal to unity at spatial periods larger than approximately 6.5 mm.

Results of the resolution measurements with the LTP-II in the 2B SLED/CCP operational mode are depicted in Fig. 16. In this case, the profiler's PSF can be precisely modeled with the two-Gaussian function, given with Eq. (4). The corresponding ITF has a phase reversal at the spatial period of approximately 3.3 mm. In this case, even at the longest available spatial periods, the value of the ITF is significantly smaller than unity. As a result, the measured amplitude of the quasi-periodic surface perturbation with the spatial period of ~8.5 mm (see the PSD spectrum in Fig. 12a) is significantly lower than that measured with the LTP-II in the single beam arrangement.

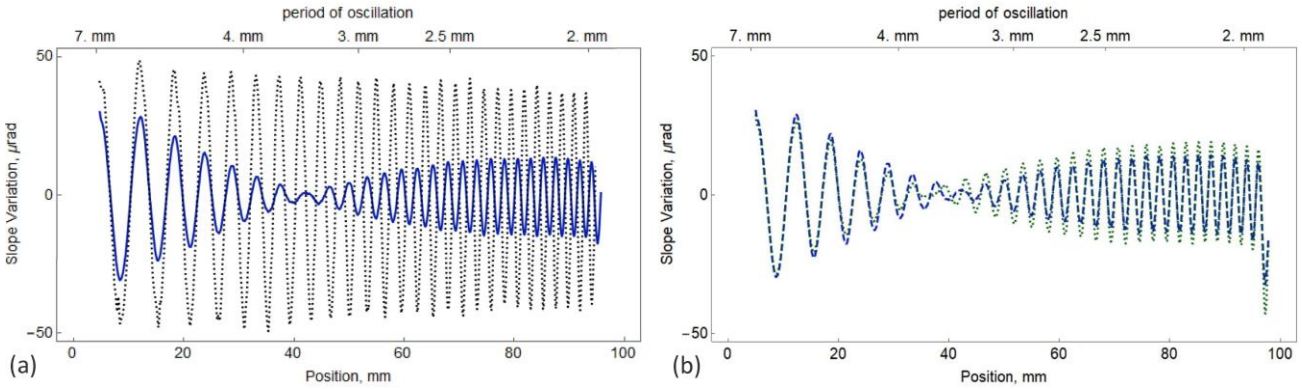

Figure 16. (a) Chirped test sample slope profile measured with the LTP-II in the 2B SLED/CCP operational mode (the solid blue line); (the dotted black line) the inherent slope variation of the low-frequency pattern of the chirped sample as measured with a Fizeau interferometer with the effective pixel size of 0.1 mm [50]; (b) the same as in plot (a) slope profile measured with the LTP-II in the 2B SLED/CCP operational mode (the dashed blue line) overlapped with the result of a similar measurement with the LTP-II in the 2B SMDL/CCP operational mode (the dotted green line). There is a noticeable difference in the chirped-test-sample slope profiles measured with the SLED and SMDL light beams over the region corresponding to the ITF with the reversed phase.

Results of the resolution measurements with the LTP-II in the 2B SLED/CCP operational mode are depicted in Fig. 16. In this case, the profiler's PSF can be precisely modeled with the two-Gaussian function, given with Eq. (4). The corresponding ITF has a phase reversal at the spatial period of approximately 3.3 mm. In this case, even at the longest available spatial periods, the value of the ITF is significantly smaller than unity. As a result, the measured amplitude of the quasi-periodic surface perturbation with the spatial period of ~8.5 mm (see the PSD spectrum in Fig. 12a) is significantly lower than that measured with the LTP-II in the single beam arrangement.

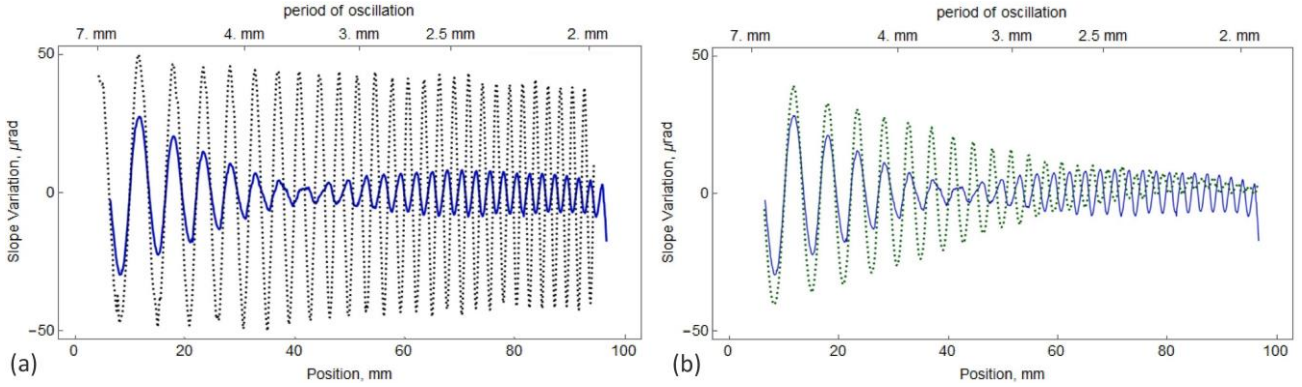

Figure 17. (a) Chirped test sample slope profile measured with the LTP-II in the 2B SLED/GMF operational mode (the solid blue line); (the dotted black line) the inherent slope variation of the low-frequency pattern of the chirped sample; (b) the same as in plot (a) slope profile measured with the LTP-II in the 2B SLED/GMF mode (the solid blue line) overlapped with the result of a similar measurement with the LTP-II in the 1B SMDL/PBI operational mode (the dotted green line).

5. CONCLUSIONS

With the aim of improving the long trace profiler at the ALS X-Ray Optics Laboratory, we have developed an original multifunctional light beam source that gives additional functional flexibility to the LTP optical sensor. We have

specifically provided detailed information on the optical schematic and design of the MFLB source to facilitate the implementation of similar sources at other metrology labs.

With this source, the LTP can be easily reconfigured for measurements of both x-ray mirrors and diffraction gratings. Usage of a light beam with a low degree of coherence for mirror metrology helps to suppress the LTP systematic errors due to spurious interference effects produced by the LTP optical elements. This conclusion is based on the comprehensive investigations of the LTP-II systematic errors in the different operational modes. We have found that for all tested options of the LTP-II metrology with a reference elliptical mirror, usage of the light beam from the superluminescent light-emitting-diode provides smaller systematic error than that of the single-mode diode-laser.

However, the SLED light source cannot support LTP-II metrology of x-ray diffraction gratings. For this class of tasks, the high-coherence narrow-band light beam from the SMDL light source is the option for groove-density-distribution characterization of diffraction gratings.

We have also performed, and first reported in this paper, a comprehensive investigation of the LTP-II spatial resolution in eight difference operational modes that are now available with the MFBS source. The major goal of the investigation, as well as the systematic error tests, was to understand if there is any advantage to using the two-beam arrangement of the profiler.

We have experimentally demonstrated that the application of the SLED light source to LTP-II measurements of x-ray mirrors results in smaller systematic error than that produced by the SMDL light source. This is probably due to the suppression of the errors due to the spurious interference effects that are more pronounced with the coherent SMDL source. We have also found that both two-beam modes utilizing the SLED light source and the 2B SMDL mode, with the CCP positioning algorithm, exhibit a null in the ITF with a phase reversal at higher spatial periods, while the one-beam modes do not exhibit this non-linear behavior.

Based on the performed systematic error and spatial resolution calibration experiments, we can come to definitive answer to this question: There is no evidence showing a preference for using the two-beam mode over the single beam mode either with the SMDL or with the SLED light beam source.

The work on numerical simulation of the experimental results of this paper, using a comprehensive optical modeling of the LTP-II, is in progress and will be discussed elsewhere.

ACKNOWLEDGEMENTS

The authors are thankful to Sergey Nikitin for useful discussions.

Research at the Advanced Light Source and the Molecular Foundry at Lawrence Berkeley National Laboratory is supported by the Office of Science, Office of Basic Energy Sciences, and Material Science Division of the U.S. Department of Energy under Contract No. DE-AC02-05CH11231.

DISCLAIMER

REFERENCES

[1] Samoylova, L., Sinn, H., Siewert, F., Mimura, H., Yamauchi, K., and Tschentscher, T., "Requirements on hard X-ray grazing incidence optics for European XFEL: Analysis and simulation of wavefront transformations," Proc. SPIE 7360, 73600E/1-9 (2009); https://doi.org/10.1117/12.822251.

[2] Cocco, D., "Recent Developments in UV optics for ultra-short, ultra-intense coherent light sources," Photonics 2015, 2(1), 40-49 (2015); https://doi.org/10.3390/photonics2010040.

[3] Idir, M. and Yashchuk, V. V., Co-Chairs, "Optical and X-ray metrology," in: X-ray Optics for BES Light Source Facilities, Report of the Basic Energy Sciences Workshop on X-ray Optics for BES Light Source Facilities, D. Mills and H. Padmore, Co-Chairs, pp. 44-55, U.S. Department of Energy, Office of Science, Potomac, MD (March 27-29, 2013); http://science.energy.gov/~/media/bes/pdf/reports/files/BES_XRay_Optics_rpt.pdf.

[4] Takacs, P. Z., "X-ray optics metrology," in: Handbook of Optics, 3rd ed., Vol. V, M. Bass, Ed., Chapter 46, McGraw-Hill, New York (2009).

[5] Takacs, P. Z., Qian, S., and Colbert, J., "Design of a long trace surface profiler," Proc. SPIE 749, 59-64 (1987); https://doi.org/10.1117/12.939842.

[6] Takacs, P. Z., Feng, S. K., Church, E. L., Qian, S., and Liu, W-M., "Long trace profile measurements on cylindrical aspheres," Proc. SPIE 966, 354-64 (1989); https://doi.org/10.1117/12.948082.

[7] Rommeveaux, A., Thomasset, M., and Cocco, D., "The Long Trace Profilers," in [Modern Developments in X-ray and Neutron Optics], A. Erko, M. Idir, T. Krist, A. G. Michette, Eds., Chapter 10, Springer-Verlag, Berlin/Heidelberg (2008).

[8] Kirschman, J. L., Domning, E. E., McKinney, W. R., Morrison, G. Y., Smith, B. V., and Yashchuk, V. V., "Performance of the upgraded LTP-II at the ALS Optical Metrology Laboratory," Proc. SPIE 7077, 70770A/1-12 (2008).

[9] Senba, Y., Kishimoto, H., Ohashi, H., Yumoto, H., Zeschke, T., Siewert, F., Goto, S., and Ishikawa, T., "Upgrade of long trace profiler for characterization of high-precision X-ray mirrors at SPring-8," Nucl. Instr. and Meth. A 616(2-3), 237-240 (2010).

[10] Siewert, F., Noll, T., Schlegel, T., Zeschke, T., and Lammert, H., "The Nanometre Optical Component Measuring Machine: a new Sub-nm Topography Measuring Device for X-ray Optics at BESSY," AIP Conference Proceedings 705, 847-850 (2004).

[11] Siewert, F., Buchheim, J., Zeschke, T., Störmer, M., Falkenberg, G., and Sankari, R., "On the characterization of ultra-precise X-ray optical components: advances and challenges in ex situ metrology," J. Synchrotron Rad. 21, 968–975 (2014); doi:10.1107/S1600577514016221.

[12] Yashchuk, V. V., Barber, S., Domning, E. E., Kirschman, J. L., Morrison, G. Y., Smith, B. V., Siewert, F., Zeschke, T., Geckeler, R., and Just, A., "Sub-microradian surface slope metrology with the ALS Developmental Long Trace Profiler," Nucl. Instr. and Meth. A 616(2-3), 212-223 (2010).

[13] Alcock, S. G., Sawhney, K. J. S., Scott, S., Pedersen, U., Walton, R., Siewert, F., Zeschke, T., Senf, F., Noll, T., and Lammert, H., "The Diamond-NOM: A non-contact profiler capable of characterizing optical figure error with sub-nanometre repeatability," Nucl. Instr. Meth. A 616(2-3), 224-228 (2010).

[14] Qian, J., Sullivan, J., Erdmann, M., Khounsary, A., and Assoufid, L., "Performance of the APS optical slope measuring system," Nucl. Instrum. and Meth. A 710, 48–51 (2013); https://doi.org/10.1016/j.nima.2012.10.102.

[15] Nicolas, J. and Martınez, J. C., "Characterization of the error budget of Alba-NOM," Nucl. Instr. and Meth. A 710, 24-30 (2013).

[16] Lacey, I., Artemiev, N. A., Domning, E. E., McKinney, W. R., Morrison, G. Y., Morton, S. A., Smith, B. V., and Yashchuk, V. V., "The developmental long trace profiler (DLTP) optimized for metrology of side-facing optics at the ALS," Proc. SPIE 9206, 920603/1-11 (2014); doi:10.1117/12.2061969.

[17] Qian, S., Geckeler, R. D., Just, A., Idir, M., and Wu, X., "Approaching sub-50 nanoradian measurements by reducing the saw-tooth deviation of the autocollimator in the Nano-Optic-Measuring Machine," Nucl. Instr. and Meth. A 785, 206-212 (2015).

[18] Lacey, I., Anderson, K., Centers, G. P., Geckeler, R. D. Gevorkyan, G. S., Just, A., Nicolot, T., Smith, B. V., and Yashchuk, V. V., "The ALS OSMS: Optical Surface Measuring System for high accuracy two-dimensional slope metrology with state-of-the-art x-ray mirrors," Proc. SPIE 10760, 1076002 (2018); https://doi.org/10.1117/12.2321347.

[19] Yashchuk, V. V., Artemiev, N. A., Lacey, I., McKinney, W. R., and Padmore, H. A., "Advanced environmental control as a key component in the development of ultra-high accuracy ex situ metrology for x-ray optics," Opt. Eng. 54(10), 104104/1-14 (2015); doi: 10.1117/1.OE.54.10.104104.
[20] Yashchuk, V. V., "Optimal Measurement Strategies for Effective Suppression of Drift Errors," Rev. Sci. Instrum. 80, 115101-1-10 (2009); http://dx.doi.org/10.1063/1.3249559.
[21] Polack, F., Thomasset, M., Brochet, S. and Rommeveaux, A., "An LTP stitching procedure with compensation of instrument errors: Comparison of SOLEIL and ESRF results on strongly curved mirrors," Nucl. Instr. and Met. A 616(2-3), 207-211 (2010).
[22] Nicolas, J., Pedriera, J., Sics, I., Ramirez, C., and Campos, J., "Nanometer accuracy with continuous scans at the ALBA-NOM," Proc. SPIE 9962, Advances in Metrology for X-Ray and EUV Optics VI, 996203 (2016); doi:10.1117/12.2238128.
[23] Yashchuk, V. V., Centers, G., Gevorkyan, G. S., Lacey, I., and Smith, B. V., "Correlation methods in optical metrology with state-of-the-art x-ray mirrors," Proc. SPIE 10612, 106120O (2018); https://doi.org/10.1117/12.2305441.
[24] Geckeler, R. D. and Just, A., "Optimized use and calibration of autocollimators in deflectometry," Proc. SPIE 6704, 670407/1-12 (2007).
[25] Yashchuk, V. V., Artemiev, N. A., Lacey, I., and Merthe, D. J., "Correlation analysis of surface slope metrology measurements of high quality x-ray optics," Proc. SPIE 8848, 88480I-1-15 (2013); doi: 10.1117/12.2024694.
[26] Geckeler, R. D. and Just, A., "A shearing-based method for the simultaneous calibration of angle measuring devices," Meas. Sci. and Tech. 25, 105009 (2014); DOI: 10.1088/0957-0233/25/10/105009.
[27] Siewert, F., Buchheim, J., and Zeschke, T., "Characterization and calibration of 2nd generation slope measuring profiler," Nucl. Instrum. Meth. A616, 119–27 (2010); doi:10.1016/j.nima.2009.12.033
[28] Alcock, S. G., Bugnar, A., Nistea, I., Sawhney, K., Scott, S., Hillman, M., Grindrod, J., and Johnson, I., "A novel instrument for generating angular increments of 1 nanoradian," Rev. Sci. Instrum. 86, 125108 (2015); http://dx.doi.org/10.1063/1.4937352.
[29] Kranz, O., Geckeler, R. D., Just, A., Krause, M., and Osten, W., "From plane to spatial angles: PTB's spatial angle autocollimator calibrator," Adv. Opt. Tech. 4(5-6), 397–411 (2015); DOI: 10.1515/aot-2015-0017.
[30] Yashchuk, V. V., Artemiev, N. A., Centers, G., Chaubard, A., Geckeler, R. D., Lacey, I., Marth, H., McKinney, W. R., Noll, T., Siewert, F., Winter, M., and Zeschke, T., "High precision tilt stage as a key element to universal test mirror for characterization and calibration of slope measuring instruments," Rev. Sci. Instrum. 87(5), 051904 (2016); doi: 10.1063/1.4950729.
[31] Qian, S., Sostero, G., and Takacs, P. Z., "Precision calibration and systematic error reduction in the long trace profiler," Opt. Eng. 39(1), 304-310 (2000); doi: 10.1117/1.602364.
[32] Geckeler, R. D., Křen, P., Just, A., Schumann, M., Krause, M., and Yashchuk, V. V., "Environmental influences on autocollimator-based angle and form metrology," Rev Sci. Instrum. 90(2), 021705/1-15 (2019); doi: 10.1063/1.5057402.
[33] MÖLLER-WEDEL OPTICAL, GmbH, "ELCOMAT 3000;" https://www.haag-streit.com/moeller-wedel-optical/products/electronic-autocollimators/elcomat-series/elcomat-3000/.
[34] Cocco, D., Sostero, G., and Zangrando, M., "Technique for measuring the groove density of diffraction gratings using the long trace profiler," Rev. Sci. Instrum. 74(7), 3544-3548 (2003); https://doi.org/10.1063/1.1584080.
[35] Thomasset, M., Dvorak, J., Brochet, S., Dennetiere, D., and Polack, F., "Grating metrology for X-ray and V-UV synchrotron beamlines at SOLEIL," Rev. Sci. Instrum. 90(2), 021714 (2019); https://doi.org/10.1063/1.5055284.
[36] Siewert, F., Lammert, H., Reichardt, G., Hahn, U., Treusch, R., and Reininger, R., "Inspection of a spherical triple VLS-grating for self-seeding of FLASH at DESY," AIP Conf. Proc. 879, 667-670 (2007); https://doi.org/10.1063/1.2436150.
[37] Centers, G., Smith, B. V., and Yashchuk, V. V., "New operational mode of the pencil beam interferometry based LTP," Proc. SPIE 9962, 996202/1-13 (2016); https://doi.org/10.1117/12.2238298.
[38] Nikitin, S. M., Gevorkyan, G. S., McKinney, W. R., Lacey, I., Takacs, P. Z., and Yashchuk, V. V., "New twist in the optical schematic of surface slope measuring long trace profiler," Proc. SPIE 10388, 103850I-1-17 (2017); https://doi.org/10.1117/12.2274400.
[39] ALS-U, https://als.lbl.gov/als-u/.
[40] Kevan, S., Chair, [ALS-U: Solving Scientific Challenges with Coherent Soft X-Rays], Workshop report on early science enabled by the Advanced Light Source Upgrade, ALS, LBNL, Berkeley, CA, (2017) https://als.lbl.gov/wp-content/uploads/2017/08/ALS-U-Early-Science-Workshop-Report-Full.pdf.

[41] Takacs, P.Z., Lacey, I., and Yashchuk, V. V., "Raytracing the Long Trace Profiler" (This conference, paper No. 11492-2, Tracking No. OP20O-OP314-12).
[42] von Bieren, K., "Pencil Beam Interferometer For Aspherical Optical Surfaces," Proc. SPIE 343, 101-108 (1982); https://doi.org/10.1117/12.933743.
[43] von Bieren, K., "Interferometry of wave fronts reflected off conical surfaces," Appl. Opt. 22, 2109-2114 (1983); https://doi.org/10.1364/AO.22.002109.
[44] von Bieren, K., "Pencil beam interferometer," US Patent 4,498,773 (1985).
[45] Irick, S. C., McKinney, W. R., Lunt, D. L. T., and Takacs, P. Z., "Using a straightness reference in obtaining more accurate surface profiles," Rev. Sci. Instrum. 63, 1436–1438 (1992); https://doi.org/10.1063/1.1143036.
[46] Irick, S. C., "Improved measurement accuracy in a long trace profiler: compensation for laser pointing instability," Nucl. Instrum. Methods Phys. Res. A 347, 226–230 (1994); https://doi.org/10.1016/0168-9002(94)91882-1.
[47] Li, H., Takacs, P. Z., and Oversluizen, T., "Vertical scanning long trace profiler: a tool for metrology of x-ray mirrors," Proc. SPIE 3152,180–187 (1997); https://doi.org/10.1117/12.295557.
[48] Takacs, P. Z., Church, E. L., Bresloff, C. J., Assoufid, L., "Improvements in the accuracy and the repeatability of long trace profiler measurements," Appl. Optics 38(25), 5468-5479 (1999); https://doi.org/10.1364/AO.38.005468.
[49] Lacey, I. and Yashchuk, V. V., "Characterization of groove density variation of VLS gratings with ALS XROL LTP-II in different operation modes" (This conference, paper No. 11492-11, Tracking No. OP20O-OP314-8).
[50] Yashchuk, V. V., Lacey, I., Arnold, T., Paetzelt, H., Rochester, S., Siewert, F., and Takacs, P. Z., "Investigation on lateral resolution of surface slope profilers," Proc. SPIE 11109, 111090M/1-19 (2019); doi: 10.1117/12.2539527.
[51] NECSEL/USHIO Diode Lasers SLM Series; https://www.ushio.com/files/specifications/necsel-slm-series-632-8-laser-diode-module.pdf
[52] Bristol Instruments 671 Series Laser Wavelength Meter Model 671B-VIS; http://www.bristol-inst.com/products/wavelengthmeters -scientific/671-series-CW-lasers.
[53] EXALOS Superluminescent Light Emitting Diodes modules; http://www.exalos.com/sled-modules/.
[54] Matuschek, N., Castiglia, A., Malinverni, M., Mounir, C., Rossetti, M., and Duelk, M., "Latest Improvements on RGB Superluminescent LEDs," NUSOD 2018, Post-deadline paper WBPD/1-2 (2018); https://www.nusod.org/2018/nusod18paperWBPD.pdf.
[55] OZ Optics digital variable attenuator DA-100; https://www.ozoptics.com/ALLNEW_PDF/APN0002.pdf.
[56] Faustini, L., and Martini, G., "Bend loss in single-mode fibers," J. Lightwave Tech. 15(4), 671-679 (1997); doi: 10.1109/50.566689.
[57] Smink, R. W., de Hon, B. P., and Tijhuis, A.G., "Bend-induced loss in single-mode fibers," Proc. Symposium IEEE/LEOS Benelux Chapter, 2005, p.p. 281-284; http://www.photonics-benelux.org/images/stories/media/proceedings/2005/s05p281.pdf.
[58] Yashchuk, V. V., Lacey, I., Gevorkyan, G. S., McKinney, W. R., Smith, B. V., and Warwick, T., "Ex situ metrology of aspherical pre-shaped x-ray mirrors at the Advanced Light Source," Rev. Sci. Instrum. 90(2), 021711 (2019); doi: 10.1063/1.5057441.
[59] Yashchuk, V. V., Rochester, S., Lacey, I., and Babin, S., "Super-resolution surface slope metrology of x-ray mirrors," Rev. Sci. Instrum. 91, 075113 (2020); doi: 10.1063/5.0005556.
[60] Yashchuk, V. V., Irick, S. C., MacDowell, A. A., McKinney, W. R., Takacs, P. Z., "Air convection noise of pencil-beam interferometer for long-trace profiler," Proc. SPIE 6317, 63170D-1-12 (2006).
[61] Siewert, F., Buchheim, J., Höft, T., Zeschke, T., Schindler, A., and Arnold, T., "Investigations on the spatial resolution of autocollimator-based slope measuring profilers," Nucl. Instrum. Methods A 710, 42–47 (2013); https://doi.org/10.1016/j.nima.2012.10.130.
[62] Siewert, F., Zeschke, T., Arnold, T., Paetzeld, H., and Yashchuk, V. V., "Linear chirped slope profile for spatial calibration in slope measuring deflectometry," Rev. Sci. Instrum. 87(5), 051907/1-8 (2016); https://doi.org/10.1063/1.4950737.
[63] Müller, H., Böhm, G., and Arnold, T., "Next generation of a linear chirped slope profile fabricated by Plasma Jet Machining," Proc. SPIE 11171, 111710A (2019); https://doi.org/10.1117/12.2526746.
[64] Boreman, G. D., [Modulation Transfer Function in Optical and Electro-optical Systems], SPIE Press, Bellingham, Washington (2001).
[65] Kay, S. M., [Modern Spectral Estimation: Theory and Application], Prentice Hall, Englewood Cliffs (1988).
[66] Jenkins, G. M. and Watts, D. G., [Spectral Analysis and its Applications], Fifth Printing: Emerson-Adams Press, Boca Raton (2007).